Deciphering the dynamics of inorganic carbon export from intertidal salt marshes using high-frequency measurements

Sophie N. Chu[a,b,1], Zhaohui Aleck Wang[b,*], Meagan Eagle Gonneea[c], Kevin D. Kroeger[c], Neil K. Ganju[c]

[a] Massachusetts Institute of Technology-Woods Hole Oceanographic Institution Joint Program in Oceanography/Applied Ocean Science and Engineering, 77 Massachusetts Avenue, Cambridge, MA 02139, USA
[b] Department of Marine Chemistry and Geochemistry, Woods Hole Oceanographic Institution, 266 Woods Hole Road, MS 8, Woods Hole, MA 02543, USA
[c] Woods Hole Coastal and Marine Science Center, U.S. Geological Survey, 384 Woods Hole Road, Woods Hole, MA 02543, USA

ABSTRACT

The lateral export of carbon from coastal marshes *via* tidal exchange is a key component of the marsh carbon budget and coastal carbon cycles. However, the magnitude of this export has been difficult to accurately quantify due to complex tidal dynamics and seasonal cycling of carbon. In this study, we use *in situ*, high-frequency measurements of dissolved inorganic carbon (DIC) and water fluxes to estimate lateral DIC fluxes from a U.S. northeastern salt marsh. DIC was measured by a CHANnelized Optical Sensor (CHANOS) that provided an *in situ* concentration measurement at 15-min intervals, during periods in summer (July – August) and late fall (December). Seasonal changes in the marsh had strong effects on DIC concentrations, while tidally-driven water fluxes were the fundamental vehicle of marsh carbon export. Episodic events, such as groundwater discharge and mean sea water level changes, can impact DIC flux through altered DIC concentrations and water flow. Variability between individual tides within each season was comparable to mean variability between the two seasons. Estimated mean DIC fluxes based on a multiple linear regression (MLR) model of DIC concentrations and high-frequency water fluxes agreed reasonably well with those derived from CHANOS DIC measurements for both study periods, indicating that high-frequency, modeled DIC concentrations, coupled with continuous water flux measurements and a hydrodynamic model, provide a robust estimate of DIC flux. Additionally, an analysis of sampling strategies revealed that DIC fluxes calculated using conventional sampling frequencies (hourly to two-hourly) of a single tidal cycle are unlikely to capture a representative mean DIC flux compared to longer-term measurements across multiple tidal cycles with sampling frequency on the order of tens of minutes. This results from a disproportionately large amount of the net DIC flux occurring over a small number of tidal cycles, while most tides have a near-zero DIC export. Thus, high-frequency measurements (on the order of tens of minutes or better) over the time period of interest are necessary to accurately quantify tidal exports of carbon species from salt marshes.

1. Introduction

Despite their small areal extent, intertidal salt marshes are a significant sink of atmospheric CO_2, with a net uptake of 4.8 ± 0.5–87.2 ± 9.6 Tg C yr^{-1} on a global scale, and an average long-term burial rate in sediments of 218 ± 24 g C m^{-2} yr^{-1} (Chmura et al., 2003; Duarte et al., 2005; McLeod et al., 2011). The outwelling hypothesis, that salt marshes are an important source of organic carbon and nutrients to the coastal ocean, has driven decades of research on carbon and nutrient cycling in these systems (Teal, 1962; Odum, 1968). More recent studies indicate that tidal marshes also export a significant amount of dissolved inorganic carbon (DIC) to adjacent waters *via* tidal exchange, such that this lateral carbon export may be an important component of the coastal carbon budget (Morris and Whiting, 1986; Cai and Wang, 1998; Raymond et al., 2000; Raymond and Hopkinson, 2003; Neubauer and Anderson, 2003; Wang and Cai, 2004).

Broadly, DIC export from coastal marshes results from production of organic matter followed by plant and microbial respiration in marsh

sediments and tidal water, and then subsequent tidal exchange with adjacent estuaries or coastal waters (Wang and Cai, 2004). These processes operate over a variety of temporal scales. Biogeochemical cycling of DIC concentrations (hereafter [DIC]) in tidal marshes is typically controlled by seasonal plant production and concurrent microbial activity (Wang and Cai, 2004; Wang et al., 2016), while tidal water fluxes vary within and between individual tidal (~12–24 h), and spring-neap (~14 d) cycles. Episodic events such as storms and groundwater inputs potentially affect carbon export from marshes, although an assessment of such effects is lacking. Indeed, while diel light and dark cycles affect photosynthesis and respiration rates, they only exert a minor control on DIC fluxes (hereafter F_{DIC}) compared to tidally-driven variability (Wang and Cai, 2004).

While mechanistic understanding of processes driving production of DIC in coastal wetlands has evolved, it has been challenging to quantify the magnitude of lateral carbon export due to the high temporal variability of hydrological (inundation, groundwater), biogeochemical (photosynthesis, respiration), and physical (light, temperature, storm activity) processes. Furthermore, the accuracy of F_{DIC} estimates is further confounded by the limitations of current methods. First, salt marsh studies have traditionally estimated carbon tidal export using sampling plans that include taking at most hourly bottle samples over a few tidal cycles on a monthly or seasonal interval (Morris and Whiting, 1986; Neubauer and Anderson, 2003; Wang and Cai, 2004). While no assessment has yet been made of what time scales (*e.g.*, tidal, spring-neap, and seasonal) must be resolved to capture the entire annual flux, it is likely that sampling a few tidal cycles does not capture the full range of concentrations or water exchange seen throughout the year, and thus may bias the seasonal or annual extrapolations, ultimately leading to large uncertainties in the contribution of wetlands to the coastal carbon budget (Duarte et al., 2005; Bouillon et al., 2008; Cai, 2011; Bauer et al., 2013; Herrmann et al., 2015; Wang et al., 2016, Najjar et al., 2018). Sparse sampling is also unlikely to capture episodic events that may potentially contribute a significant portion of the overall flux. Second, if water fluxes are estimated from the tidal prism, rather than directly measured, they may not fully capture the magnitude or timing of water flux in these complex environments (Gardner et al., 2006). Large extrapolations between sampling events to generate seasonal or annual estimates of export could therefore result in large uncertainties (Downing et al., 2009; Ganju et al., 2012).

A recently published study by Wang et al. (2016) demonstrated that high-frequency sampling and directly measured water flow captured the temporal variability of both biogeochemical and hydrological processes and may have greatly reduced the F_{DIC} uncertainty. In the 2016 study, we used data from seasonal bottle sampling over tidal cycles and *in situ* high-frequency biogeochemical sensors in a multiple linear regression (MLR) model to estimate high-frequency [DIC]. Concentrations were then combined with high-frequency measurements of tidal flow and modeled water fluxes to generate high-frequency instantaneous F_{DIC}. Based on this high-frequency method, Wang et al. (2016) estimated an annual F_{DIC} export of 414 g C m^{-2} from a salt marsh in the northeast U.S.. This export was more than twice the previously estimated F_{DIC} in U.S. southeastern marshes (Neubauer and Anderson, 2003; Wang and Cai, 2004). Wang et al. (2016) suggested that such a large difference potentially resulted from the fact that the MLR method was able to capture much more variability in [DIC] and water fluxes over tidal, seasonal, and annual time scales, including episodic events and high-frequency tidal variability. They concluded that conventional discrete sampling may not be able to capture the true dynamics of marsh tidal exports that span such a wide range of time scales, each of which is highly variable.

In this study, we build on our previous work in Wang et al. (2016) by deploying a recently developed *in situ* DIC sensor, CHANnelized Optical System (CHANOS) (Wang et al., 2015), along with a suite of other physical and biogeochemical sensors, to directly quantify high-frequency F_{DIC} in a salt marsh tidal creek during the summer and fall of

2015. While the study site is the same as the previous study, this is the first time that high-frequency, direct measurements of [DIC] and water fluxes were measured simultaneously over significant periods of time in a salt marsh with the aim to accurately assess lateral DIC exports. Additionally, we evaluated the robustness and validity of the MLR method from Wang et al. (2016) to determine whether accurate estimates of [DIC] require direct measurements by a specialized sensor like CHANOS or whether they could be estimated by an MLR based on more readily available parameters verified with periodic [DIC] discrete bottle sampling. With CHANOS's high-frequency (15-min) data, we provide an in-depth analysis of directly measured DIC export at tidal and seasonal timescales as well as a comparison of the effectiveness of conventional sampling frequencies to resolve the true magnitude of lateral DIC fluxes over a specific interval.

2. Materials and methods

2.1. Study site

Sage Lot Pond (SLP) is an intertidal salt marsh located near the eastern inlet of Waquoit Bay, on Cape Cod, Massachusetts (Fig. 1). As stated in Wang et al. (2016), SLP is comparable to other Atlantic salt marshes with respect to faunal and floral communities and is typical for a New England salt marsh, with regard to relative sea level rise rate (2.81 ± 0.18 mm yr^{-1}, based on monthly mean sea level from 1932 to 2015, NOAA Tide Station ID 8447930), and mean annual temperature (9.88 °C) (Chmura et al., 2003). It has a small, forested watershed that delivers a relatively low level of nutrient loading, estimated at ~12 kg N ha^{-1}yr^{-1} (Kroeger et al., 2006).

A time-series sampling site was established at the mouth of a tidal creek that drains a well-constrained portion of the marsh where both discrete sampling and high-frequency *in situ* sensor measurements were obtained. The drainage area (Fig. 1b) was defined using a 1-m bare-earth LiDAR-derived digital elevation model (DEM), and a water drop analysis routine (Wang et al., 2016). Elevation range for the marsh was 0 to 0.3 m. Maximum tidal amplitude ranged from −0.4 to 0.4 m. The drainage basin associated with the chosen tidal creek site has an area of 4132 m^2, excluding ponds, with fresh groundwater discharge comprising a minor portion of the water budget (see details in section 2.4 Assessment of water fluxes). This area was used to determine area-normalized fluxes from the salt marsh.

2.2. Discrete sampling and analysis

Discrete bottle samples were collected at ~30 cm above the bottom of the tidal creek every 1–2 h at the sampling site using a peristaltic or diaphragm pump for periods of a full tidal cycle (~12–14 h) in April, July, October, November, and December in 2015. These samples from 2015 were not included in the Wang et al. (2016) study, which covered the period from 2012 to 2014. DIC collection and analysis followed standard best practice procedures outlined by Dickson et al. (2007). Samples were collected through purgeable capsule filters with 0.45 μm pore size (Farrwest Environmental Supply, Texas, USA) into 250 mL borosilicate bottles, poisoned with 100 uL saturated mercuric chloride, sealed with a glass stopper coated with APIEZON® – L grease, and secured with a rubber band.

Discrete bottle samples were measured with an Apollo SciTech DIC auto-analyzer (Model AS-C3) by acidifying the sample with 10% phosphoric acid. The acidified CO_2 sample was purged with high purity nitrogen gas and total CO_2 gas was detected with a LICOR-7000 infrared analyzer (LI-COR Environmental, Nebraska, USA). Certified Reference Material (CRM) from Dr. A.G. Dickson at the Scripps Institution of Oceanography was used to calibrate the DIC auto-analyzer. DIC values were reported in μmol kg^{-1} after being corrected for water density and mercuric chloride addition. The precision and accuracy of the instrument is ± 2.0 μmol kg^{-1} (one standard deviation)
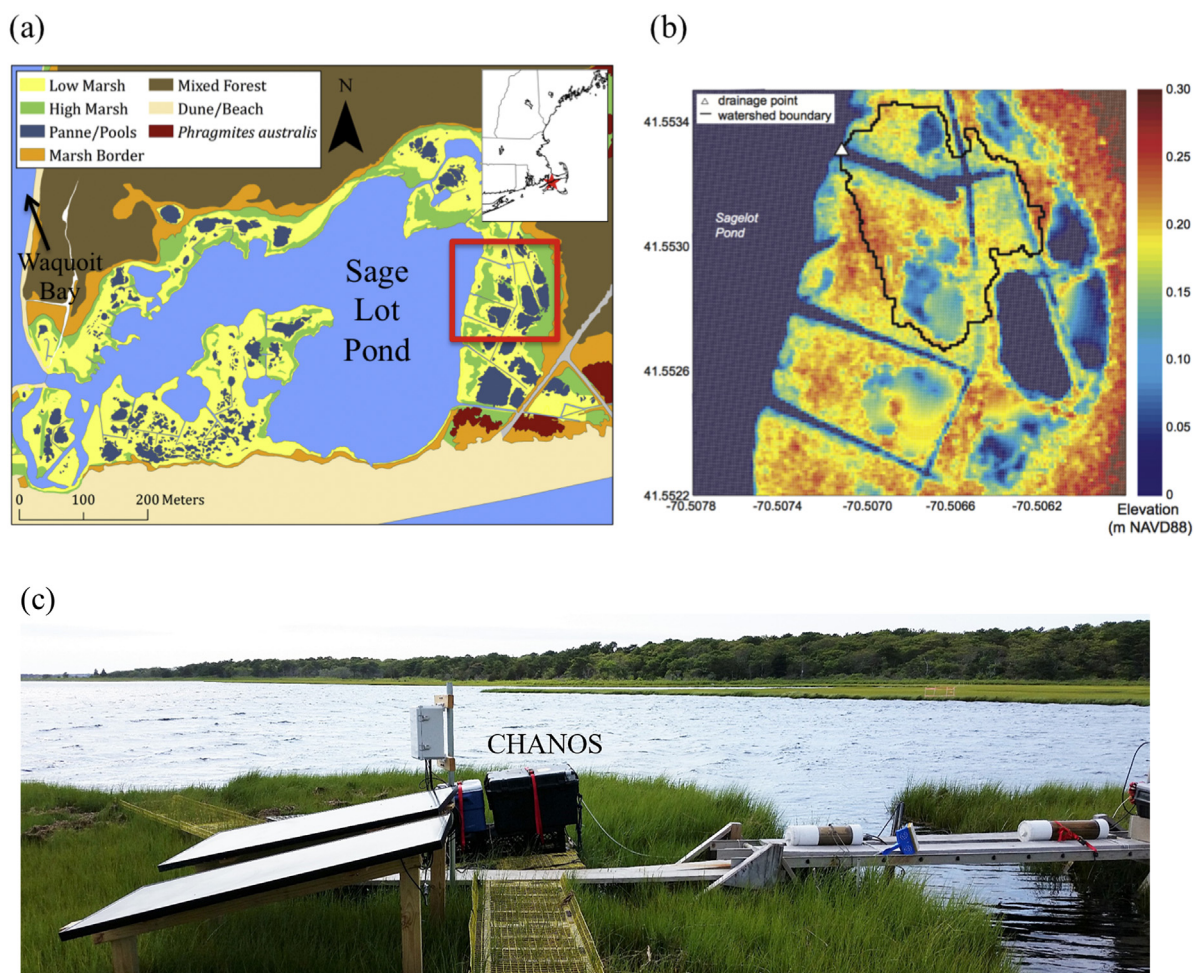
Fig. 1. (a) The Sage Lot Pond marsh sampling area with habitat classifications, (b) the drainage basin (elevation indicated by colour map) for the time-series sampling tidal creek (small triangle as the sampling site), and (c) the picture showing the CHANelized Optical Sensor (CHANOS) deployment setup in Waquoit Bay National Estuarine Research Reserve (WBNERR) on Cape Cod, Massachusetts. The red rectangle in (a) represents the area containing the drainage basin outlined in black in panel (b). Map in (a) was created by WBNERR with habitat classifications based on 2004 aerial photography (NIR, 0.25 m resolution). Water boundary layer was provided by MassGIS. (For interpretation of the references to colour in this figure legend, the reader is referred to the web version of this article.)

estimated based on replicate measurements and inter-laboratory comparison of CRM measurements (Bockmon and Dickson, 2015) using the sampling protocol described above.

2.3. High-frequency sensor measurements

In situ high-frequency sensors were deployed at the SLP tidal creek to measure physical and biogeochemical properties of tidal water from April to December 2015. An EXO2 Multiparameter Sonde (YSI Inc., Yellow Springs, OH) measured temperature, salinity, water depth, dissolved oxygen (DO), fluorescent dissolved organic matter (fDOM), chlorophyll, turbidity, oxidation/reduction potential (ORP), and probe pH. In this study, we only use the salinity (measured on the practical salinity scale), DO (measured in percentage of saturation), and ORP (measured in mV) parameters from the EXO2. A SonTek IQ Plus acoustic Doppler velocity meter (ADVM) (Sontek/YSI, San Diego, CA) measured water velocity and surface elevation. The YSI EXO2 recorded at intervals ranging from 2 min to 8 min and the Sontek IQ recorded time-averaged data every 15 min. The relative elevation of the deployed Sontek IQ was referenced to NAVD88 and is associated with negligible error. All EXO2 sensors were cleaned and calibrated regularly according to manufacturer recommended methods to maintain performance, and antifouling measures were deployed including copper and automated wiping. After a deployment period of 2–4 weeks, YSI EXO2 data for

2015 were evaluated for fouling and calibration drift, similar to Wang et al. (2016) YSI data from 2012 to 2014. The YSI EXO2 was recalibrated and a correction factor based on calibration standards was applied linearly across the deployment as needed. A maximum correction up to ± 30% of the calibration value was allowed or otherwise discarded (Wagner et al., 2006); however, the 30% threshold was only exceeded for one parameter (ORP) during one deployment. During the 13 deployments, DO was corrected during one period (1.4%), ORP was corrected during 5 periods (1–30%) and salinity was corrected during 3 periods (maximum correction 0.2 salinity units). Reported YSI EXO2 sensor accuracy specifications are: 0.20 pH units (NBS scale), 1% of the reading for salinity, 0.05 °C for temperature, 1% of the reading for dissolved oxygen, and 20 mV for ORP.

The Sontek IQ ADVM includes a vertical beam and integrated pressure sensor to measure water level in addition to four transducers with two along-axis beams and two skew beams to measure velocity. Sontek IQ ADVM proprietary software internally calculates cross-sectional area with user-provided creek geometry and Sontek IQ measured water depth. Cross-sectional area is then multiplied by mean channel velocity to provide flow in and out of the creek. The uncertainty in water flux arising from cross-sectional area and velocity measurement as well as internal algorithms is reported as < 5%.

In addition to the Sontek IQ and YSI EXO2, an *in situ* CHANOS sensor (Wang et al., 2015) was also deployed at the tidal creek sampling

site in July – August and December 2015. CHANOS was placed on a platform atop the marsh adjacent to the creek with the inlet pumping from the creek at the same depth and within 30 cm of the YSI (Fig. 1c). This setup avoided any interference by CHANOS on water flow in the creek. There is no significant concentration difference with depth in the creek (data not shown). In order to prevent fouling, sample water was filtered by a 100 μm plastic disc filter (Keller Products, Acton, MA) followed by a copper mesh filter. CHANOS was powered by two 12 V batteries that were charged with two 250 W solar panels (Renogy, Ontario, CA).

CHANOS uses spectrophotometric principles to measure DIC and pH using two independent channels (Wang et al., 2015). Briefly, CHANOS consisted of syringe pumps for delivery of reagents, junction boxes containing valves, thermistors, and optical and fluidic components for DIC and pH analysis, and an electronics housing, as well as reagent bags for storage of CRM, hydrochloric acid, reference solution, and pH-sensitive indicator solution. For this study, only [DIC] measurements were used. The DIC channel uses an improved spectrophotometric method described in detail in Wang et al. (2013) whereby a counter-current flow configuration between acidified seawater and a pH-sensitive indicator solution in a tube-in-tube design achieves fast, continuous CO_2 equilibration across highly CO_2-permeable Teflon AF 2400 tubing. After CO_2 exchange in the countercurrent flow cell, the indicator solution is directed into an optical cell for detection. A spectrophotometer measures the absorbance at the wavelengths for indicator acid and base species, and the absorbance ratio (R) is used to calculate the final [DIC] concentration using Eq. 4 from Wang et al. (2015):

$$log\frac{[DIC]}{(K_0)_a} = B(t) - log(K_0)_i - log\left(\frac{R - e_1}{1 - R\frac{e_3}{e_2}}\right) \tag{1}$$

here, $(K_0)_i$ is the Henry's Law constant for the internal indicator solution, $(K_0)_a$ is the Henry's Law constant for the acidified sample calculated using salinity from the YSI EXO2 and temperature measured by the CHANOS, e_1, e_2, e_3 are indicator molar absorbance ratios, and $B(t)$ is a calibration constant determined by measuring CRM at specific temperatures. Each measurement cycle is ~15 min. The system achieved a precision of $\sim \pm 2.5\,\mu mol\,kg^{-1}$ and an accuracy of $\sim \pm 5.0\,\mu mol\,kg^{-1}$ during coastal deployments (Wang et al., 2015).

CHANOS was calibrated autonomously both in the laboratory and *in situ* with CRM over the range of temperatures at which field measurements were conducted. CHANOS [DIC] measurements were corrected based on discrete bottle samples (Supporting information Fig. S1). Discrete bottle samples were collected over 2–3 days during each CHANOS deployment in July and December. Bottle samples were matched to CHANOS measurements taken within 8 min of each other. After correction, the mean residual between CHANOS and bottle measurements was $0 \pm 44\,\mu mol\,kg^{-1}$ with $n = 30$ and $r^2 = 0.86$ for all points.

Possible sources of larger uncertainty ($\pm 44\,\mu mol\,kg^{-1}$) compared to the reported [DIC] error for CHANOS ($\pm 5.0\,\mu mol\,kg^{-1}$, Wang et al., 2015) may include the following: 1) [DIC] data processing requires actual measurement temperature. The CHANOS instrument was deployed on the marsh surface outside the tidal creek to avoid impacting water fluxes. Consequently, the actual measurement temperature by CHANOS might not be equal to *in situ* water temperature as is the case for typical in-water deployment. Air temperature was measured by a thermistor near the measurement cell, and it was treated as the CHANOS measurement temperature. The actual measurement temperature is likely between *in situ* water temperature and air temperature. Many factors contributed to this temperature difference, such as time of day, season, or weather conditions. Every degree Celsius difference in temperature would result in a difference in [DIC] of $7–9\,\mu mol\,kg^{-1}$. The average temperature difference between the CHANOS air temperature and YSI water temperature was ~4.5 °C, which would result in a [DIC] offset of $30–40\,\mu mol\,kg^{-1}$. Although the actual measurement temperature was likely in between the CHANOS

and YSI, this temperature difference could account for a large portion of the uncertainty between [DIC] measured by the CHANOS and discrete bottle samples. 2) All constants in Eq. 1 vary with salinity. Properly aligning the YSI EXO2 salinity measurements to CHANOS measurements and CHANOS measurements to discrete bottle samples could cause uncertainty, especially if the water flow was large and caused the water composition to be slightly different in between CHANOS and bottle sampling times. 3) The composition (alkalinity) of the indicator solution used for CHANOS [DIC] measurements could change over time if storage bags are compromised, thus causing calibration errors in [DIC] measurements. This is likely a minor error compared to temperature discrepancy because indicator solution bags were replaced ~monthly and the impermeable laminated bags have been shown to be stable within a three-week field test (Wang et al., 2015).

2.4. Assessment of water fluxes

Water fluxes were calculated using the methodology described in Wang et al. (2016). Briefly, SonTek IQ ADVM water fluxes measured in the tidal creek were used to derive the base (raw) water fluxes. Corrections were made to the base SonTek IQ water fluxes to account for overland flow and groundwater contributions to the marsh creek. Overland flow occurs when tidal height is above the marsh surface and flooding or ebbing tidal water inundates or drains the marsh without going through the creek channel. Water flow over the marsh is not measured by the ADVM and therefore needs to be accounted for with a correction. The ratio between the flow in the tidal creek and the total tidal flux in the marsh drainage basin depends on tidal height and the platform elevation. To correct for overland flow in order to assess total tidal flux in the drainage area at a given time, a hydrodynamic model was created for the drainage basin of the tidal creek to derive such ratios using the 1-m DEM with the Coupled Ocean-Atmosphere-Wave-Sediment Transport (COAWST) model (Warner et al., 2010). Flood and ebb corrections were each determined from the ratio of water fluxes in the tidal creek to total water fluxes during flood or ebb conditions, respectively, and then applied to the measured ADVM water fluxes in the creek channel to derive total tidal fluxes as a function of water level and flow direction (Wang et al., 2016). The hydrodynamic model does not include any mechanisms controlling carbon cycling as its purpose is to correct overland flow in order to obtain high-frequency tidal fluxes.

We also included a groundwater correction to the DIC fluxes. Groundwater can affect DIC fluxes in two ways, by contributing both a water flux component and a [DIC] component. Assuming the annual net tidal flow should be zero, the mean water flow over the study period was shifted to match to the net groundwater flow as described in further detail in Wang et al. (2016). The annual net groundwater flow was estimated to be $0.00024\,m^3\,s^{-1}$ or $7570\,m^3\,yr^{-1}$ calculated using the isohaline method from MacCready (2011) and the salt balance application from Ganju (2011). The correction shift to match the mean flow to the net groundwater flow was $0.0017\,m^3\,s^{-1}$ ($5.36 \times 10^4\,m^3\,yr^{-1}$). This is only 3% of the mean annual tidal flow magnitude ($0.057\,m^3\,s^{-1}$ or $1.8 \times 10^6\,m^3\,yr^{-1}$), suggesting that groundwater flow is only a small fraction of net tidal water flux at this site.

Finally, total tidal water flux (Q) was used in combination with [DIC] concentrations to calculate instantaneous DIC flux (F_{DIC}):

$$F_{DIC} = [DIC]*Q \tag{2}$$

We assume that the [DIC] measured at the tidal creek sampling site is representative of the [DIC] entering and exiting the drainage area such that F_{DIC} represents the total DIC flux into and out of the drainage basin at any given moment.

2.5. Multiple linear regression DIC model

A multiple linear regression (MLR) model was developed using discrete [DIC] bottle measurements and *in situ* YSI EXO2 parameters to

Table 1
Coefficients and associated standard errors used for the DIC multiple linear regression.

	Intercept	Day'	Sal. (PSS-78)	DO (% saturation)	ORP (mV)	n	R²	RMSE
DIC (µmol kg⁻¹)	557 ± 58	73.2 ± 9.9	57.7 ± 2.6	−3.5 ± 0.3	−0.5 ± 0.1	104	0.91	58

estimate high-frequency [DIC] concentrations similar to the method used in Wang et al. (2016) at the same location. Data used for the MLR covered the time period from April to December 2015 when discrete bottle and YSI EXO2 measurements were taken. The chosen parameters to characterize [DIC] were Day', salinity (S), dissolved oxygen (DO), and oxidation-reduction potential (ORP) resulting in the following equation to predict [DIC]:

$$[DIC](umol\ kg^{-1}) = k + a(Day') + b(S) + c(pH) + d(ORP) \quad (3)$$

where Day' = $\sin\left(\frac{2\pi Jday}{365}\right)$, and Jday is Julian Day, a value between 1 and 365. The Day' term accounts for seasonal cycling, where January is treated similarly to December and February (Lefevre et al., 2005; Friedrich and Oschlies, 2009; Signorini et al., 2013). The [DIC] MLR coefficients (Table 1) were optimized for the highest correlation coefficient (R^2) and lowest root mean square error (RMSE). Parameters were chosen based on data availability, data quality, and goodness of fit. Salinity characterizes mixing effects of the estuary and marsh water on [DIC]. DO and ORP represent the effects of aerobic and anaerobic respiration processes that occur in the marsh sediments and water. The MLR was able to capture [DIC] variability at 91% with an RMSE of 58 µmol kg⁻¹.

2.6. Mean tide calculations

High-frequency time-series measurements allowed for evaluation of mean characteristics of a tidal cycle for each of the two measurement periods by CHANOS, July–August and December 2015. That data treatment reveals representative features within a tidal cycle and mean seasonal differences, and the ability of different sampling strategies to capture a 'representative' mean tidal cycle for flux estimates (see Section 3.6). A mean tidal cycle over ~12.42 h for each period was constructed based on high-frequency CHANOS data. Individual tidal cycles were first divided into 15-minute intervals (the frequency of time-series measurements for [DIC]) with the starting point from the time of lowest water level (low tide). Measured parameters, estimated DIC fluxes, and water fluxes were then binned into 15-minute intervals over each tidal cycle, and then each bin was averaged across all tides within each of the two periods to create a July – August and December representative mean tide.

2.7. Error analysis for DIC flux estimates

Uncertainty in DIC flux estimates was assessed using Monte Carlo simulations with the maximum uncertainty possible. A Monte Carlo simulation was run for the MLR [DIC] by adding a random error to each value of the input parameters based on their respective uncertainties, where a 5% error was assumed for Day (seasonal variability), and other uncertainties were from the YSI EXO2 manual, 1% for S, 1% for DO, and 20 mV for ORP. 1000 iterations were generated for each time point for MLR [DIC] with random errors and the average [DIC] and standard deviation was found for each point. Averaged over all time points, the standard deviation was < 1% of the average [DIC]. For CHANOS [DIC], the overall uncertainty was 44 µmol kg⁻¹ based on comparison to discrete bottle samples or 2% using the Monte Carlo analysis. For [DIC]

errors, 58 µmol kg⁻¹ and 44 µmol kg⁻¹ were used for MLR and CHANOS uncertainty, respectively. To estimate error in the calculation of F_{DIC}, uncertainty was first added to base fluxes based on the water flow measurement uncertainty from the ADVM at 5%. Then, we assumed random errors centered at 25% for the flood and ebb equations for the overland corrected fluxes and a random error with the same magnitude as the groundwater correction (0.0017 m³ s⁻¹) was added to corrected fluxes, such that the total uncertainty included error from measured base water fluxes as well as the overland and groundwater corrections to the water fluxes.

3. Results and discussion

3.1. High-frequency time series CHANOS [DIC] measurements

Our conceptual model is that [DIC] in the tidal creek is mainly affected by biogeochemical cycling in the marsh and the creek water, and mixing between water sources including estuary, marsh drainage, and fresh groundwater. High-frequency MLR and CHANOS [DIC] measurements captured the combined effect of these contributing factors. The CHANOS was deployed in July 7 – August 11 and November 30 – December 18, 2015 (Fig. 2). In July – August (Fig. 2a–b), CHANOS [DIC] showed a clear tidal signal. At high tide, [DIC] was close to the estuarine end member at ~1800–1900 µmol kg⁻¹. [DIC] at low tide reached values of ~2200–2400 µmol kg⁻¹, due to the addition of CO_2 from respiration of marsh organic carbon in sediments and creek water. These concentrations were similar to the ranges of discrete [DIC] bottle samples reported for July and August of 2012–2014 in Wang et al. (2016). Water temperatures during this period had a daily cycle ranging from 20 to 30 °C (Fig. 2b). Salinity stayed relatively constant between 28 and 32 ppt with lowest salinities at low tide. Most of this small salinity variability may be due to the limited input of groundwater at this site. Water level showed a clear tidal cycle with one high-high tide and one low-low tide over a day. It ranged from −0.4 to +0.4 m at spring tides and −0.1 to +0.25 m at neap tides when the tidal range was smallest (Fig. 2b).

In contrast to July – August, [DIC] during regular tidal cycles in December (Fig. 2c) showed a smaller variation range of ~100 to 200 µmol kg⁻¹ over a tidal cycle compared to ~400 to 600 µmol kg⁻¹ seen in July – August. The smaller tidal [DIC] range in November 30 – December 18 is likely a result of reduced respiration in the salt marsh and tidal creek. However, the difference between maximum and minimum concentrations observed in this period (~1200–2100 µmol kg⁻¹) were similar to the range in July – August, since the period of December 4–9 had the lowest [DIC] (~1200–1500 µmol kg⁻¹) observed. This period also corresponded to a drop in salinity from ~30 to as low as 15 and the lowest water level, close to −0.4 m, in December (Fig. 2c–d).

In general, there was much more variability in salinity in December compared to July – August, with a few low tides where salinity was below 20 (Fig. 2d). There were more rain events in December compared to July – August (Fig. 2); however, there did not appear to be a consistent effect of rainfall on [DIC]. Lower [DIC], more variable salinity, and lower water levels likely indicate influence from groundwater inputs. Groundwater [DIC] at this site range from 1040 to 2570 µmol kg⁻¹ (Wang et al., 2016). Lower sea level in this period compared to July – August (Fig. 2) might increase the hydraulic gradient from land to sea, driving an increase in the rate of groundwater discharge (Gonneea et al., 2013).

3.2. CHANOS DIC fluxes over two study periods

Overland and groundwater corrected CHANOS F_{DIC} in July – August 2015 showed large variability and a clear tidal cycle signal (Fig. 3). In general, tidal cycles of F_{DIC} were smaller in December 2015. There was a period of time (December 4–9) when F_{DIC} were close to zero (Fig. 3).
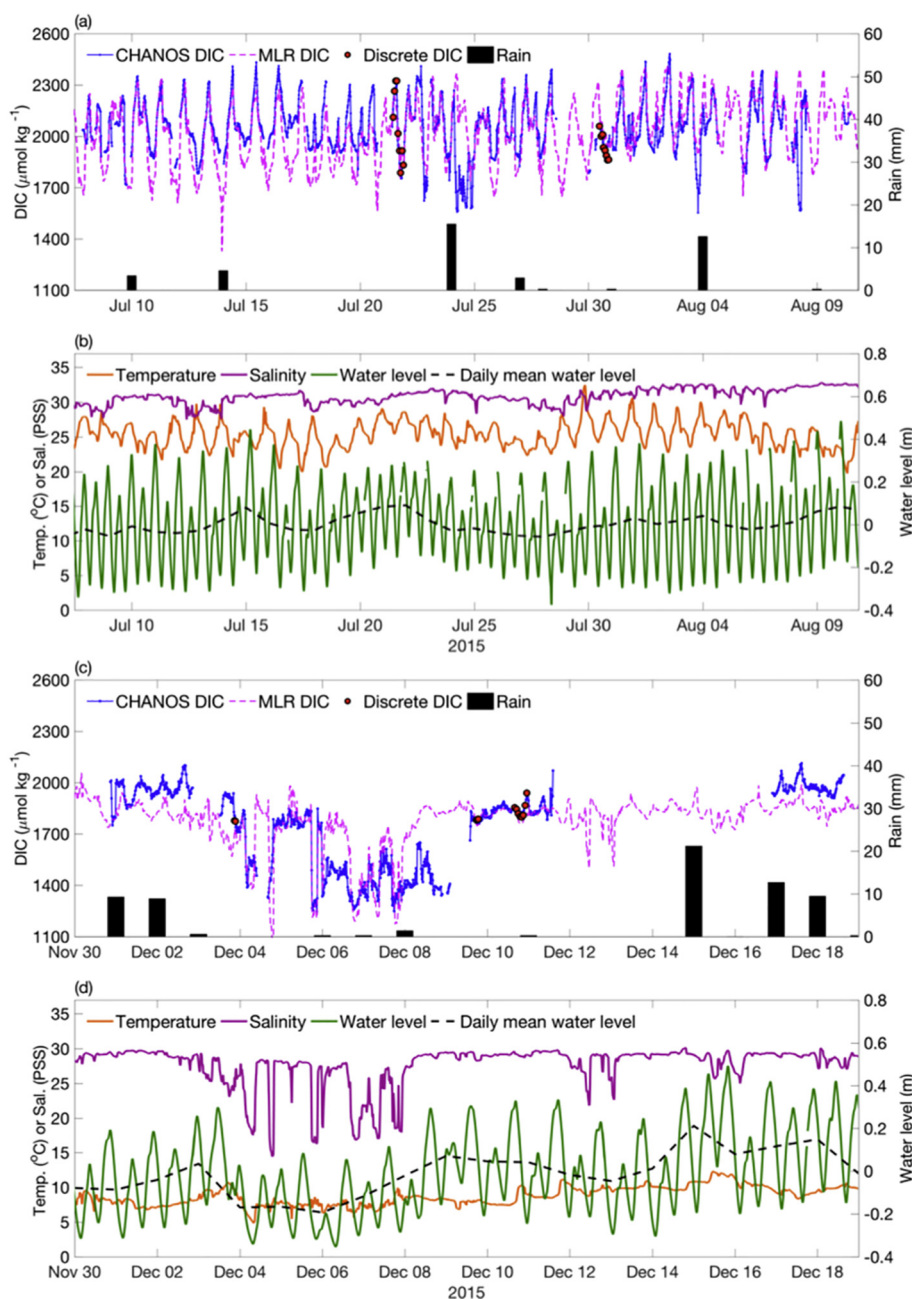
Fig. 2. Time series measurements of biogeochemical and environmental parameters at the Sage Lot Pond marsh tidal creek from 2015. CHANOS measured DIC, MLR modeled DIC, discrete bottle DIC samples and precipitation are shown from a) July – August and c) December. b) and d) show corresponding temperature (°C), salinity (PSS), and water level (m) referenced to NAVD88 in the two sampling periods. Rain data are from NOAA NERRS, n.d.

This corresponds to low [DIC], salinity decrease, and low water levels (Fig. 2). The low water level decreased water flow during this period, which may result in an insignificant F_{DIC}. Larger F_{DIC}, comparable in magnitude to those in July – August of ~ -10 to $10\,g\ C\ s^{-1}$, only occurred from December 15–18, likely driven by a period of larger water fluxes, shown by the water level ranging from -0.2 to $0.4\,m$ (Fig. 2).

Mean F_{DIC} base flux for CHANOS was $-0.26\,g\ C\ s^{-1}$ (1973 g C $m^{-2}\,yr^{-1}$) for July – August and $-0.17\,g\ C\ s^{-1}$ (1284 g C $m^{-2}\,yr^{-1}$) for December (Table 2). The Monte Carlo analysis as described earlier resulted in an uncertainty of ~12% for the CHANOS base F_{DIC} over both periods and ~47% uncertainty for final corrected fluxes, where ~30% of the uncertainty is due to errors in the measured water flow and the

remainder due to overland and groundwater corrections. After corrections for overland flow and groundwater inputs, the mean F_{DIC} rate based on CHANOS data was about 25% greater in July 7 – August 11 compared to November 30 – December 18 (Table 2). In July – August, the overland flow correction reduced the mean F_{DIC} significantly by 0.07 g C s^{-1} (558 g C $m^{-2}\,yr^{-1}$) or ~28%. Similarly, in December the correction was 0.04 g C s^{-1} (260 g C $m^{-2}\,yr^{-1}$) or ~20%. The overland correction in these two periods was generally in line with that of Wang et al. (2016). The groundwater water flux correction decreased seaward export by ~0.03–0.04 g C s^{-1} in both months. Due to infrequent sampling, groundwater [DIC] input was unable to be estimated at the same frequency to match F_{DIC} in order to make corrections to F_{DIC}. Such a mismatch in temporal resolution might introduce additional

Fig. 3. Time series of DIC fluxes calculated using water fluxes and either CHANOS measured DIC or MLR estimated DIC in (a) July–August and (b) December. Positive values indicate the direction of flux is into the marsh and negative flux values indicate export to the coast.

uncertainty in the groundwater correction. The contribution of [DIC] by direct groundwater discharge accounted for < 10% of the total corrected annual flux at SLP (Wang et al., 2016).

The corrected mean CHANOS F_{DIC} showed an export rate of 1084 g C $m^{-2} yr^{-1}$ (converted to an annual flux rate for comparison) in July – August and 743 g C $m^{-2} yr^{-1}$ in December (Table 2). These 2015 exports are higher, especially in July – August, than those found in Wang et al. (2016) using the MLR modeling method derived from the data collected in 2012–2014 (July – August export of 500–550 g C $m^{-2} yr^{-1}$ and December export of < 400 g C $m^{-2} yr^{-1}$). Several possible reasons may explain the differences of the monthly mean fluxes between the two studies. In this study, CHANOS measurements only covered a portion of July and December, and thus the derived monthly rate may not be representative of full monthly means. The monthly mean DIC fluxes estimated from Wang et al. (2016) were averaged over multiple months from three years. It is unlikely that this difference in flux magnitude is due to differences in the methods since this study demonstrates that base DIC fluxes as well as overland and groundwater corrected mean F_{DIC} calculated using MLR estimated [DIC] are comparable to those estimated from the CHANOS measurements, which suggests the validity of the two methods (Table 2; see details in the following section).

3.3. Comparison of CHANOS and MLR [DIC] concentrations and corresponding fluxes

To verify whether the MLR method could be used as a robust method to estimate DIC exports from the marsh, MLR derived DIC concentrations and fluxes were compared directly to CHANOS measured [DIC] and derived F_{DIC} for both sampling periods (Figs. 4 and 5). In July – August, taking a simple mean of the residuals between MLR and CHANOS [DIC] (MLR [DIC] – CHANOS [DIC]) at each time point resulted in an average difference of -23 ± 154 (one standard deviation) μmol kg^{-1} ($N = 2470$). Applying the Monte Carlo simulation method discussed in section 2.7 by adding random errors to MLR and CHANOS [DIC] resulted in a similar mean [DIC] residual between MLR and CHANOS of $-24 \pm 49 \mu$mol kg^{-1}. For July – August, the residuals were mostly randomly distributed over the CHANOS [DIC] concentration range, except for several points at either extreme, where the MLR overestimated at low CHANOS [DIC] and the MLR underestimated at high CHANOS [DIC] (Fig. 4a). [DIC] residuals > 500 μmol kg^{-1} also occurred at high salinity between 31 and 33 ppt (Fig. 4c), when water flows were close to zero (Fig. 4e). Two large rain events on July 24 and August 4 (Fig. 2a) showed > 500 μmol kg^{-1} differences between MLR

Table 2
Mean CHANOS and MLR estimated DIC fluxes (reported in g C s^{-1} and converted to annual flux units in g C $m^{-2} yr^{-1}$ in parentheses) over the same time periods in the July–August and December. Negative fluxes indicate export from the marsh. Number of days covered refers to total amount of time in days when instantaneous CHANOS DIC flux was available for a given period. Missing data were not interpolated.

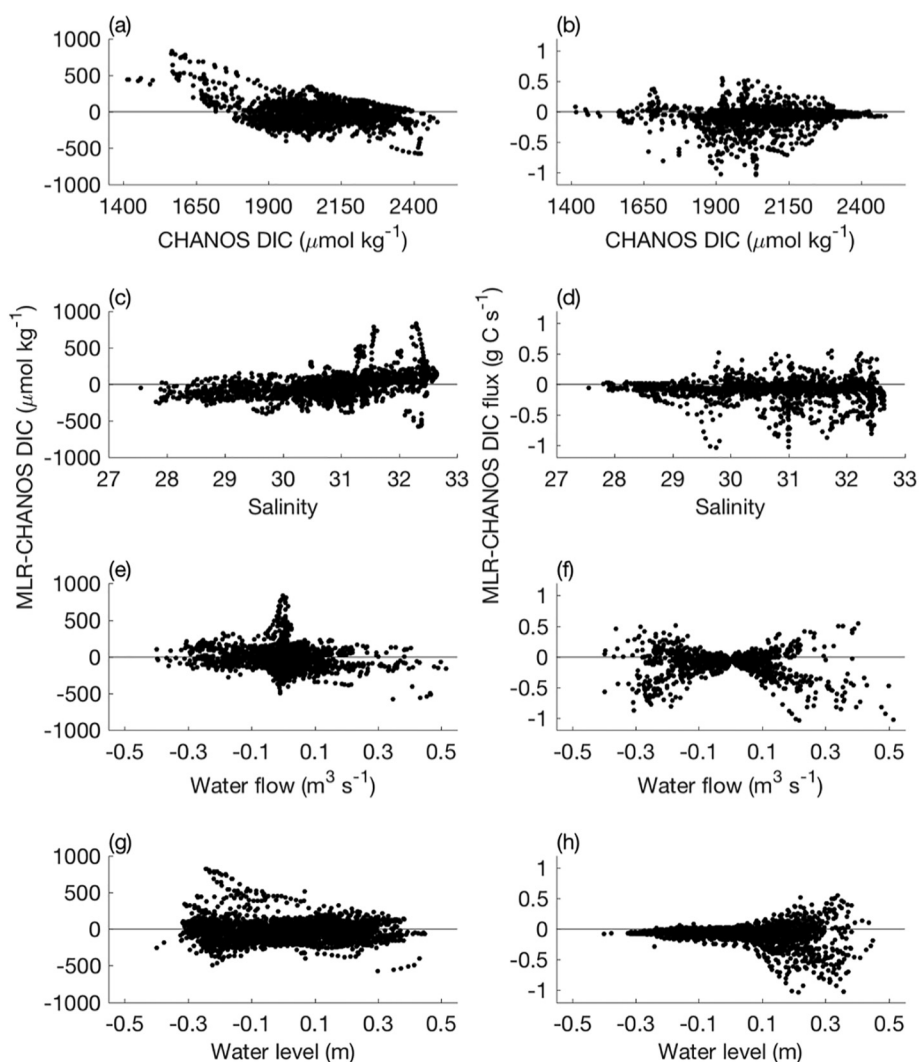| Time period	DIC base flux		DIC flux overland corrected		DIC flux overland and groundwater corrected		Number of days covered
	g C s^{-1}		g C s^{-1}		g C s^{-1}		
	(g C $m^{-2} yr^{-1}$)		(g C $m^{-2} yr^{-1}$)		(g C $m^{-2} yr^{-1}$)		
	CHANOS	MLR	CHANOS	MLR	CHANOS	MLR	
July 7 to August 11 (36 days)	−0.26	−0.28	−0.19	−0.22	−0.14	−0.17	25.7 (71% of time period)
	(−1973)	(−2159)	(−1415)	(−1648)	(−1084)	(−1321)	
November 30 to December 18 (19 days)	−0.17	−0.16	−0.13	−0.13	−0.10	−0.09	10.8 (57% of time period)
	(−1284)	(−1220)	(−1023)	(−958)	(−743)	(−679)	

July-August 2015

Fig. 4. Residuals of DIC concentration and DIC flux between MLR estimated and CHANOS measured (or derived) values (MLR – CHANOS) against CHANOS DIC concentration (a and b), salinity (c and d), water flow (e and f), and water level (g and h) in July – August 2015.

and CHANOS [DIC], where CHANOS measured lower [DIC]. The MLR model for [DIC] was established using discrete bottle samples that were collected during periods mostly without rain. Therefore, the effect of rain on [DIC] concentrations might not be fully captured by the MLR, which may result in the larger residuals. However, the patterns of differences in [DIC] did not transfer to the residuals between CHANOS and MLR F_{DIC} (Fig. 4b, d, f, and h), mostly because water flow was small during periods near slack tide when [DIC] discrepancies were large (Fig. 4e). The F_{DIC} residuals increased with water level and absolute water flux (Fig. 4f and h). This resulted from the fact that the largest absolute fluxes (both positive and negative) occurred near high tide (Fig. 4f and h). If there is a [DIC] difference between MLR and CHANOS, the difference would be magnified after multiplying [DIC] by a larger water flux. Similar to CHANOS F_{DIC} error, the MLR F_{DIC} error analysis resulted in a 16% uncertainty for MLR base fluxes, which increased to 46% after adding uncertainty from the water flux measurement uncertainty and corrections. The mean difference between MLR and CHANOS F_{DIC} was -0.03 ± 0.20 (one standard deviation) g C s^{-1}, which was about 22% of the total corrected CHANOS F_{DIC} in July – August (Table 2). Results from the Monte Carlo error analysis for MLR

and CHANOS F_{DIC} showed a mean difference in F_{DIC} of -0.03 ± 0.04 g C s^{-1} (1σ, including all uncertainties), or ~22% of the corrected CHANOS F_{DIC} for this period. As such, on average, the two methods agree reasonably well.

In December, the mean [DIC] residual between MLR and CHANOS values was $-3 \pm 172 \, \mu mol \, kg^{-1}$ or $-3 \pm 48 \, \mu mol \, kg^{-1}$ using a Monte Carlo simulation ($N = 1037$). A few large discrepancies in [DIC] residuals were mostly associated with low salinity (~15) (Fig. 5c) likely due to groundwater inputs (Figs. 2c and 5a). Rain events in December corresponded to higher CHANOS [DIC] than MLR-estimated [DIC], in contrast to July – August. The [DIC] residuals in December were also greater at high salinity and near-zero water flows (Fig. 5c and e), similar to July – August. In contrast to July–August, the residuals of F_{DIC} in December were more scattered at high salinity (Fig. 5d). The mean residual between MLR and CHANOS F_{DIC} was -0.008 ± 0.15 g C s^{-1}, about 9% of the CHANOS F_{DIC} during this period (Table 2). Monte Carlo analysis gave a mean residual of -0.013 ± 0.032 g C s^{-1}, about 13% of the CHANOS F_{DIC}, showing that there is agreement between the two methods of estimating fluxes for this period.

In summary, the MLR [DIC] model is reasonably robust, except for
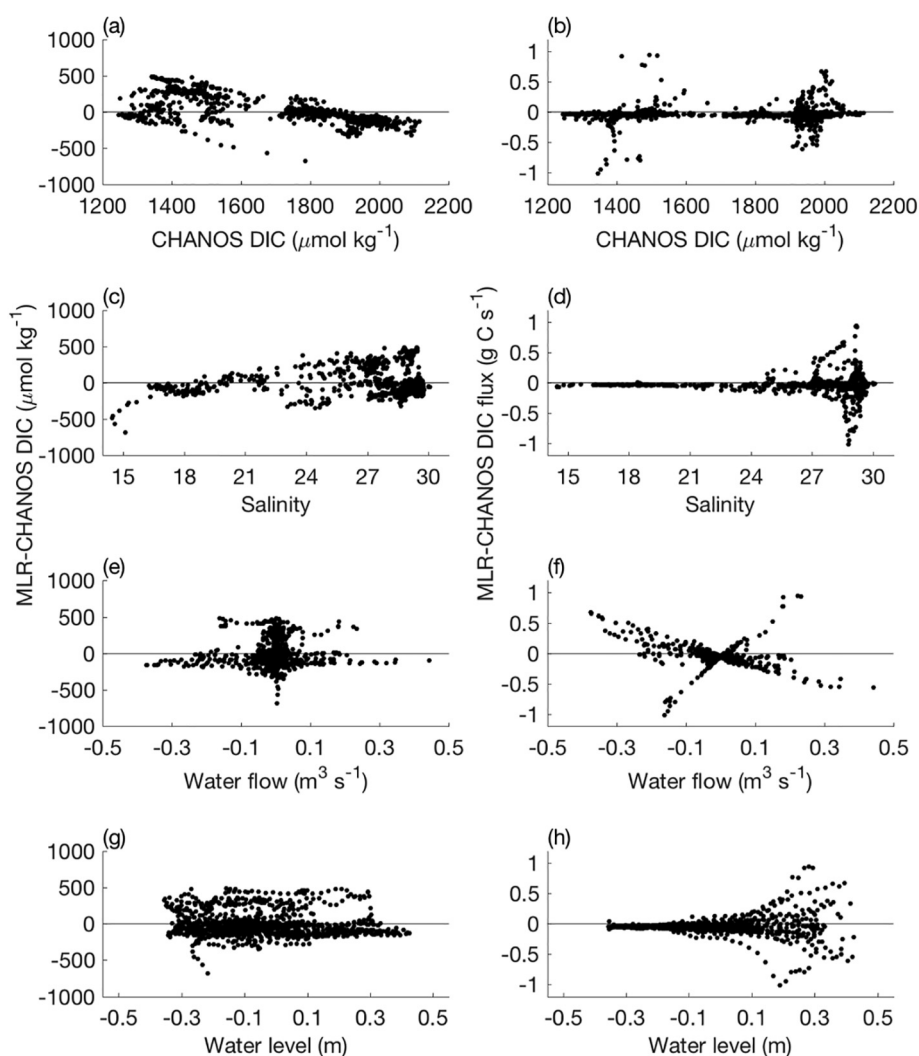
December 2015

Fig. 5. Residuals of DIC concentration and DIC flux between MLR estimated and CHANOS measured (or derived) values (MLR – CHANOS) against CHANOS DIC concentration (a and b), salinity (c and d), water flow (e and f), and water level (g and h) in December 2015.

near slack tide and periods of episodic events such as rain, which were not captured well by the MLR model. Nevertheless, such discrepancies did not greatly affect the estimates of net mean F_{DIC} in the two study periods, where the mean difference between CHANOS and MLR fluxes were < 25% of the CHANOS corrected flux for both periods. The larger uncertainty in CHANOS [DIC] measurements did not significantly affect F_{DIC} estimates due to randomness of the errors, which affected both positive and negative fluxes that partially cancel each other, as shown in this and the previous study at this site (Wang et al., 2016). Overall, using the MLR method to estimate F_{DIC} is a reasonable approach to quantify lateral transport of carbon from this salt marsh location if direct, high-frequency DIC measurements are not available.

3.4. Mean tidal cycles and variabilities of individual tides

[DIC] over the mean tidal cycle in July – August was much higher than that in December (Fig. 6a), at both high and low tide, supporting the notion that the rate of DIC generation is greater during the summer, both in the estuary and in the marsh. The mean [DIC] in the summer had a range of 2000 μmol kg^{-1} at incoming tide to 2200 μmol kg^{-1} at ebbing tide, while December showed limited variation in mean [DIC]

over a tidal cycle, varying between 1750 and 1800 μmol kg^{-1}. This result is qualitatively consistent with previous studies based on observations from limited individual tides at different seasons, suggesting strong seasonality in marsh production and respiration that are directly related to DIC production in marshes (*e.g.*, Raymond et al., 2000; Neubauer and Anderson, 2003; Wang and Cai, 2004; Wang et al., 2016). However, the analysis also showed that the variability (shaded area in Fig. 6a) in [DIC] within each period could be as large as the mean variability between the two periods at ~200–250 μmol kg^{-1}. Thus, it is likely that sampling a few individual tides in multiple seasons may not be representative of mean seasonal differences in such a dynamic environment.

There was a typical difference of ~0.4 m between mean high and low tide water levels (Fig. 6b), where July – August had a higher tidal range than December on average. Correspondingly, July – August had larger mean water fluxes (Fig. 6c), and those larger water fluxes were partially responsible for larger mean F_{DIC} in July – August (Fig. 6d). Instantaneous, CHANOS-derived F_{DIC} over the mean tidal cycle in July – August ranged from −4 to 4 g C s^{-1} compared to only −2 to 2 g C s^{-1} in December (Fig. 6d). The differences in water flux, in addition to differences in [DIC] concentration over the mean tidal cycles during
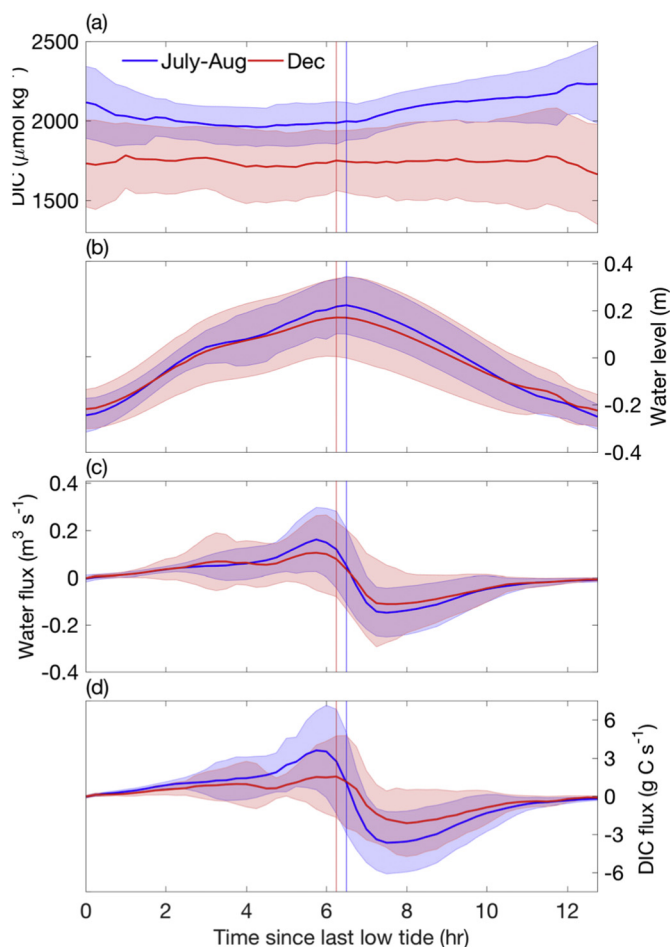
Fig. 6. Mean DIC concentration (a), water level (b), water flux (c), and DIC flux (d) over a binned tidal cycle in July – August 2015 (blue) and December 2015 (red). Shaded blue and red areas show the corresponding standard deviation of the mean values and vertical lines designate mean time for high tide for each period. The data in each period from Fig. 2 are binned every 15 min to produce means and standard deviation for each time interval over the ~12.42 h mean tide cycle. (For interpretation of the references to colour in this figure legend, the reader is referred to the web version of this article.)

these two periods, resulted in the overall difference in mean F_{DIC} (-0.20 vs. -0.15 g C s^{-1}; Table 2). Again, variability within each measurement period in terms of water level, water flux, and DIC flux are comparable to the mean variability between the July – August and December periods. The analysis also shows that on average the largest DIC fluxes (in absolute values) occur within ~2 h before and after high tide when water fluxes have peaked (Fig. 6c–d).

3.5. Effectiveness of sampling strategies to capture representative tidal cycle fluxes

In previous salt marsh studies, carbon fluxes were commonly derived using discrete samples collected over one or a few individual tidal cycles with a fixed sampling interval (e.g., hourly), along with tidal prism estimates of water exchange. These individual flux estimates for specific tidal cycles were then extrapolated to a longer time period (e.g., a month or a season) to evaluate the net flux for that period. Several concerns arise from the assumptions made by this approach. First, there has been no analysis of the sampling frequency required to capture the entire flux over a tidal cycle. Secondly, the variability in fluxes from multiple tidal cycles across months or seasons has not been constrained to determine if a tidal cycle could be representative of a longer time period. The extended time-scale and high-frequency of the

Table 3

Probabilities for different sampling protocols to capture the net DIC flux for each individual tide within 25% of the CHANOS value (where the CHANOS flux is treated as the reference or 'true' flux) during the two study periods. For a given sampling protocol, the probability is calculated as the percentage of individual tides where the DIC flux estimated from that particular sampling protocol was within 25% of the net CHANOS DIC flux over that tidal cycle. All sampling protocols are centered at high tide to attempt to balance the incoming and outgoing water fluxes whereas starting at low tide would produce a positive bias due to the variability of the length of each tidal cycle.

	12-h sampling with a 15-min interval*	8-h sampling with a 15-min interval	12-h sampling with a 60-min interval	12-h sampling with a 120-min interval
July 7 to August 11	88%	22%	36%	17%
November 30 to December 18	92%	35%	27%	15%

* 12 h was used to represent a full tidal cycle while the actual tidal period for each individual tide varied between 10.25 and 13.5 h, where tidal cycles were delineated by time of low tide to the following low tide.

measurements in this study can help to shed light on the validity of these assumptions.

To investigate the first assumption, that the tidal cycle is sampled at sufficiently high frequency with bottle samples to capture the true flux, four sampling strategies were assessed to determine the probability of obtaining a flux within 25% of the measured (CHANOS) DIC flux at each individual tide in both periods. Herein, CHANOS DIC flux was treated as the representative or actual flux. Each tide in each period was assessed by these four strategies: Case 1) 12-h sampling with a 15-min interval, Case 2) 8-h sampling with a 15-min interval, Case 3) 12-h sampling with a 1-h interval, and Case 4) 12-h sampling with a 2-h interval (Table 3). If sampling occurs at 15-min intervals over a complete tidal cycle (~12 h), in 88–92% of individual tides for the July – August and December time periods resulting flux estimates would be within 25% of their corresponding CHANOS fluxes (Table 3). Although the Case 1 sampling strategy mirrors the one employed by CHANOS, it does not capture the real flux 100% of the time. This is due in part to variability in tidal cycle periods, which range from 10.25 to 13.5 h during the study, while a fixed 12-h sampling was used for this analysis. If the sampling duration for each tide is reduced to 8 h with 15-min intervals, only 22–33% of the tides have their estimated fluxes within 25% of the actual fluxes measured. Since the sampling is centered at high tide, this result suggests that sampling a few hours right before and after a low tide when water fluxes are lowest is just as important as sampling around high tide, when water fluxes are highest. At hourly sampling over 12 h, only 27–36% of the tides would yield a mean F_{DIC} within 25% of the actual CHANOS mean flux. The probability of capturing a representative flux drops even further to 15–17% if the sampling interval doubles to every two hours over each tidal cycle. This analysis thus demonstrates that coarse sampling intervals and sampling over a shortened tidal cycle will result in inaccurate flux estimates and highlights the need for high-frequency measurements over the entire tidal cycle to more accurately determine carbon fluxes from salt marshes.

To assess the validity of the second assumption, whether or not the flux derived from an individual tide is representative of the mean flux over an extended period, we conducted a frequency analysis of all mean F_{DIC} over individual tidal cycles for the two sampling periods (Fig. 7). In July – August, the largest portion (32%) of individual mean F_{DIC} occurred in the range of -0.1–0 g C s^{-1} (small net export). The histogram flux distribution is centered at this range, following an approximately normal distribution. The tides in this range can be called 'typical' tidal cycles, when there is statistically the highest likelihood that a tidal
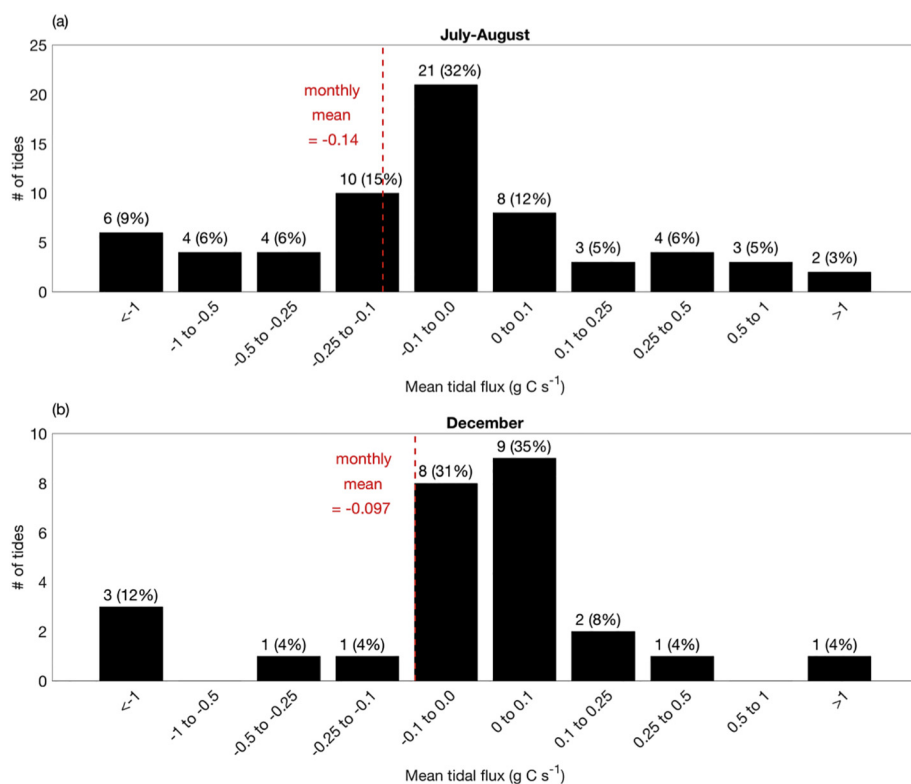
Fig. 7. Histogram distributions of mean CHANOS DIC fluxes over individual tides during the two study periods a) July–August and b) December. The overall mean DIC fluxes over the two periods are indicated in red. (For interpretation of the references to colour in this figure legend, the reader is referred to the web version of this article.)

cycle with this mean flux would be sampled and extrapolated for the entire extended time period. However, the actual mean flux over the period was $-0.14\,\text{g C s}^{-1}$, greater in export magnitude than the center of the -0.1–$0\,\text{g C s}^{-1}$ range. This mismatch was primarily driven by the fact that about 15% of the tides had much larger mean export fluxes ($<-0.5\,\text{g C s}^{-1}$) (Fig. 7). These large fluxes may result from an episodic event such as a very large tide or rain that enhances flushing of the marsh subsurface. Although CHANOS captured several episodic large flux events, there were some measurement gaps in which the MLR approach indicated that large fluxes occurred (*e.g.*, following a rain event on December 15; Figs. 2d and 3b). As such, periodic bottle sampling would almost certainly result in failure to capture episodic large flux events, thus causing an underestimate of the mean DIC flux over the entire period.

We saw a similar pattern in December, where about 31% and 35% of the tides had mean fluxes in the range of -0.1–$0\,\text{g C s}^{-1}$ and 0–$+0.1\,\text{g C s}^{-1}$, respectively. However, because of a few large export fluxes, the overall mean flux over the period was $-0.10\,\text{g C s}^{-1}$, which was significantly higher in export magnitude than the center of the flux frequency distribution in December (Fig. 7). In summary, the majority of tides have a small mean tidal flux, typically sea-ward. However, a small portion of large flux events can have a disproportionately large influence on the mean flux over a longer period. As such, it is unlikely that sampling over one or a few tidal cycles will capture a representative mean flux for an extended period. It is likely then that infrequent, low frequency sampling of tidal fluxes from salt marshes would not capture the true flux and, in fact, the failure to capture large, episodic events would result in underestimating fluxes on longer time scales (*e.g.*, monthly, seasonally and annually). This conclusion may support and provide an explanation for the high rate of DIC export ($\sim$414 gC m^{-2} yr^{-1}) estimated in the Wang et al. (2016) study, that was about twice the rate estimated in previous studies. Those previous studies were based on lower frequency and shorter duration measurements, which we have shown here are likely to underestimate total annual flux. High-frequency measurements over the period of interest are thus necessary in order to accurately measure lateral carbon fluxes in tidal marshes.

4. Conclusions

High-frequency *in situ* measurements of [DIC] and water flux allow the most direct and accurate way to quantify lateral DIC exports from salt marshes *via* tidal exchange. They also reveal the intricacies of such exports over tidal cycles at different periods over the year. The results indicate that tidally-driven water fluxes are fundamental drivers of marsh carbon export. Additionally, episodic events (*e.g.*, rain and large tides) and groundwater inputs can leave significant imprints on both DIC concentrations and fluxes at times. Direct observations confirm that there are distinct differences in [DIC], water fluxes, and F_{DIC} in mean tidal cycles in different seasons. However, the variability of F_{DIC} across tidal cycles within a season was comparable to the mean variability between seasons. The effectiveness or probability of accurately capturing the net F_{DIC} for a single tidal cycle decreases quickly with decreased sampling frequency from every 15 min up to 2 hourly sampling. Sampling incomplete tidal cycles also significantly decreases the likelihood of capturing accurate DIC fluxes. A small number of tides with high net flux accounted for a disproportionately large fraction of the mean seaward F_{DIC}, while a large portion of tides only show small DIC exports from the marsh. Insufficient sampling of these 'pulsing' events can directly cause underestimates of lateral carbon export from tidal marshes. These results highlight the need for long-term, high-frequency measurements and/or modeling to quantify tidal exports of carbon species from salt marshes.

The study concludes that using the MLR method to derive high-frequency [DIC] and thus F_{DIC} is a reasonably robust approach to define DIC export fluxes from the salt marsh in this study and offers guidance to expand this approach to other coastal wetlands. There were times when the MLR model did not show good agreement with directly measured [DIC], especially during episodic events. During these periods, the MLR model showed limited capability, likely because the discrete bottle samples used to establish the MLR model did not fully cover such events. However, net F_{DIC} were in general less sensitive to uncertainty in [DIC], as random errors tended to cancel out when estimating net fluxes by integrating positive and negative instantaneous

fluxes. In addition, much of the discrepancy between the MLR and direct [DIC] measurements occurred near slack tide when water flow was close to zero. Thus, there were limited effects on the calculation of net DIC fluxes.

Overall, this study demonstrates that highly variable lateral export of carbon species from tidal marshes can be quantified in a robust way, through both direct, high-frequency measurements or high-frequency MLR modeling, thus improving our ability to study the carbon budgets in coastal wetlands and coastal oceans.

Appendix A. Supplementary data

Supplementary data to this article can be found online at https://doi.org/10.1016/j.marchem.2018.08.005.

References

Bauer, J.E., Cai, W.J., Raymond, P.A., Bianchi, T.S., Hopkinson, C.S., Regnier, P.A.G., 2013. The changing carbon cycle of the coastal ocean. Nature 504, 61–70. https://doi.org/10.1038/nature12857.

Bockman, E.E., Dickson, A.G., 2015. An inter-laboratory comparison assessing the quality of seawater carbon dioxide measurements. Mar. Chem. 171, 36–43.

Bouillon, S., Borges, A.V., Castañeda-Moya, E., Diele, K., Dittmar, T., Duke, N.C., Kristensen, E., Lee, S.Y., Marchand, C., Middelburg, J.J., Rivera-Monroy, V.H., et al., 2008. Mangrove production and carbon sinks: a revision of global budget estimates. Global Biogeochem. Cycles 22 (2). https://doi.org/10.1029/2007GB003052.

Cai, W.J., 2011. Estuarine and coastal ocean carbon paradox: CO2 sinks or sites of terrestrial carbon incineration? Annu. Rev. Mar. Sci. 3, 123–145. https://doi.org/10.1146/annurev-marine- 120709-142723.

Cai, W.J., Wang, Y., 1998. The chemistry, fluxes, and sources of carbon dioxide in the estuarine waters of the Satilla and Altamaha Rivers, Georgia. Limnol. Oceanogr. 43, 657–668. https://doi.org/10.4319/lo.1998.43.4.0657.

Chmura, G.L., Anisfeld, S.C., Cahoon, D.R., Lynch, J.C., 2003. Global carbon sequestration in tidal, saline wetland soils. Glob. Biogeochem. Cycles 17 (doi: 1029/2002GB00191).

Dickson, A.G., Sabine, C.L., Christian, J.R., 2007. Guide to Best Practices for Ocean CO2 Measurements. PICES Special Publication.

Downing, B.D., Boss, E., Bergamaschi, B.A., Fleck, J.A., Lionberger, M.A., Ganju, N.K., Schoellhamer, D.H., Fujii, R., et al., 2009. Quantifying fluxes and characterizing compositional changes of dissolved organic matter in aquatic systems in situ using combined acoustic and optical measurements. Limnology and Oceanography 7 (1), 119–131. https://doi.org/10.4319/lom.2009.7.119.

Duarte, C.M., Middelburg, J.J., Caraco, N., 2005. Major role of marine vegetation on the oceanic carbon cycle. Biogeosciences 2, 1–8. https://doi.org/10.5194/bg-2-1-2005.

Friedrich, T., Oschlies, A., 2009. Neural networkbased estimates of North Atlantic surface pCO2 from satellite data: A methodological study. J. Geophys. Res. Oceans 114. https://doi.org/10.1029/2007JC004646.

Ganju, N.K., 2011. A novel approach for direct estimation of fresh groundwater discharge to an estuary. Geophys. Res. Lett. 38. https://doi.org/10.1029/2011GL047718.

Ganju, N.K., Hayn, M., Chen, S.N., Howarth, R.W., Dickhudt, P.J., Aretxabaleta, A.L., Marino, R., 2012. Tidal and groundwater fluxes to a shallow, microtidal estuary: constraining inputs through field observations and hydrodynamic modeling. Estuaries Coast. 35, 1285–1298. https://doi.org/10.1007/s12237-012-9515-x.

Gardner, L.R., Kjerfve, B., Petrecca, D.M., 2006. Tidal fluxes of dissolved oxygen at the North Inlet-Winyah Bay National Estuarine Research Reserve. Estuar. Coast. Shelf Sci. 67 (3), 450–460.

Gonneea, M.E., Mulligan, A.E., Charette, M.A., 2013. Climate-driven sea level anomalies modulate coastal groundwater dynamics and discharge. Geophys. Res. Lett. 40, 2701–2706. https://doi.org/10.1002/grl.50192.

Herrmann, M., Najjar, R.G., Kemp, W.M., Alexander, R.B., Boyer, E.W., Cai, W.J., Griffith, P.C., Kroeger, K.D., McCallister, S.L., Smith, R.A., et al., 2015. Net ecosystem production and organic carbon balance of U.S. East Coast estuaries: a synthesis approach. Global Biogeochem. Cycle 29 (1), 96–111. https://doi.org/10.1002/2013GB004736.

Kroeger, K.D., Cole, M.L., Valiela, I., 2006. Groundwater-transported dissolved organic nitrogen exports from coastal watersheds. Limnol. Oceanogr. 51, 2248–2261. https://doi.org/10.4319/lo.2006.51.5.2248.

Lefevre, N., Watson, A.J., Watson, A.R., 2005. A comparison of multiple regression and neural network techniques for mapping in situ pCO2 data. Tellus B 57, 375–384. https://doi.org/10.1111/j.1600-0889.2005.00164.x.

MacCready, P., 2011. Calculating estuarine exchange flow using isohaline coordinates. J. Phys. Oceanogr. 41, 1116–1124. https://doi.org/10.1175/2011JPO4517.1.

McLeod, E., Chmura, G.L., Bouillon, S., Salm, R., Björk, M., Duarte, C.M., Lovelock, C.E., Schlesinger, W.H., Silliman, B.R., 2011. A blueprint for blue carbon: toward an improved understanding of the role of vegetated coastal habitats in sequestering CO2. Front. Ecol. Environ. 9 (10), 552–560. https://doi.org/10.1890/110004.

Morris, J.T., Whiting, G.J., 1986. Emission of gaseous carbon-dioxide from salt-marsh sediments and its relation to other carbon losses. Estuaries 9, 9–19. https://doi.org/10.2307/1352188.

Najjar, R.G., Herrmann, M., Alexander, R., Boyer, E.W., Burdige, D., Butman, D., Cai, W.-J., Canuel, E.A., Chen, R.F., Friedrichs, M.A.M., Feagin, R.A., Griffith, P., Hinson, A.L., Holmquist, J.R., Hu, X., Kemp, W.M., Kroeger, K.D., Mannino, A., McCallister, S.L., McGillis, W.R., Mulholland, M.R., Pilskaln, C., Salisbury, J., Signorini, S., St-Laurent, P., Tian, H., Tzortziou, M., Vlahos, P., Wang, Z.A., Zimmerman, R.C., 2018. Carbon budget of tidal wetlands, estuaries, and shelf waters of Eastern North America. Glob. Biogeochem. Cycles 32, 389–416. https://doi.org/10.1002/2017GB005790.

Neubauer, S.C., Anderson, I.C., 2003. Transport of dissolved inorganic carbon from a tidal freshwater marsh to the York River estuary. Limnol. Oceanogr. 48, 299–307. https://doi.org/10.4319/lo.2003.48.1.0299.

NOAA National Estuarine Research Reserve System (NERRS) System-Wide Monitoring Program. Data accessed from the NOAA NERRS Centralized Data Management Office website. http://www.nerrsdata.org/, Accessed date: 12 October 2016.

Odum, E.P., 1968. Energy flow in ecosystems – a historical review. Am. Zool. 8, 11–18. https://doi.org/10.1093/icb/8.1.11.

Raymond, P.A., Hopkinson, C.S., 2003. Ecosystem modulation of dissolved carbon age in a temperate marsh-dominated estuary. Ecosystems 6, 694–705. https://doi.org/10.1007/s10021-002-0213-6.

Raymond, P.A., Bauer, J.E., Cole, J.J., 2000. Atmospheric CO2 evasion, dissolved inorganic carbon production, and net heterotrophy in the York River estuary. Limnol. Oceanogr. 45, 1707–1717.

Signorini, S.R., Mannino, A., Najjar, R.G., Friedrichs, M.A., Cai, W.J., Salisbury, J., Wang, Z.A., Thomas, H., Shadwick, E., 2013. Surface ocean pCO2 seasonality and sea-air CO2 flux estimates for the North American east coast. J. Geophys. Res. 118 (10), 5439–5460.

Teal, J.M., 1962. Energy flow in the salt marsh ecosystem of Georgia. Ecology 43, 614–624. https://doi.org/10.2307/1933451.

Wagner, R.J., Boulger, R.W.J., Oblinger, C.J., Smith, B.A., 2006. Guidelines and standard procedures for continuous water-quality monitors: station operation, record computation, and data reporting. United States Geological Survey Tech. Meth. 1-D3, 51.

Wang, Z.A., Cai, W.J., 2004. Carbon dioxide degassing and inorganic carbon export from a marsh-dominated estuary (the Duplin River): a marsh CO2 pump. Limnol. Oceanogr. 49, 341–354. https://doi.org/10.4319/lo.2004.49.2.0341.

Wang, Z.A., Chu, S.N., Hoering, K.A., 2013. High-frequency spectrophotometric measurements of total dissolved inorganic carbon in seawater. Environ. Sci. Technol. 47, 7840–7847. https://doi.org/10.1021/es504893n.

Wang, Z.A., Sonnichsen, F.N., Bradley, A.M., Hoering, K.A., Lanagan, T.M., Chu, S.N., Hammar, T.R., Camilli, R., 2015. In situ sensor technology for simultaneous spectrophotometric measurements of seawater total dissolved inorganic carbon and pH. Environ. Sci. Technol. 49, 4441–4449. https://doi.org/10.1021/es504893n.

Wang, Z.A., Kroeger, K.D., Ganju, N.K., Gonneea, M.E., Chu, S.N., 2016. Intertidal salt marshes as an important source of inorganic carbon to the coastal ocean. Limnol. Oceanogr. 61, 1916–1931. https://doi.org/10.1002/lno.10347.

Warner, J.C., Armstrong, B., He, R.Y., Zambon, J.B., 2010. Development of a coupled ocean-atmosphere-wave-sediment transport (COAWST) modeling system. Ocean Model. Online 35, 230–244. https://doi.org/10.1016/j.ocemod. 2010.07.010.